THE ASTROPHYSICAL JOURNAL, 509:768–784, 1998 December 20
© 1998. The American Astronomical Society. All rights reserved. Printed in U.S.A.

MOLECULAR ABUNDANCE ENHANCEMENTS IN THE HIGHLY COLLIMATED BIPOLAR OUTFLOW BHR 71

GUIDO GARAY AND IVE KÖHNENKAMP
Departamento de Astronomía, Universidad de Chile, Casilla 36-D, Santiago, Chile; guido@das.uchile.cl
TYLER L. BOURKE[1]
School of Physics, University College, The University of New South Wales, Australian Defence Force Academy, Canberra, ACT 2600, Australia; and Harvard-Smithsonian Center for Astrophysics, 60 Garden Street, MS 42, Cambridge, MA 02138
L. F. RODRÍGUEZ
Instituto de Astronomía, UNAM, Apdo. Postal 70-264, 04510 México D.F., México
AND
KIMMO K. LEHTINEN
Helsinki University Observatory, Tähtitorninmäki, P.O. Box 14, SF-00014, University of Helsinki, Finland; kklehtin@cc.helsinki.fi
Received 1998 May 6; accepted 1998 July 27

ABSTRACT

We report observations of the $J = 3 \rightarrow 2$ and $J = 2 \rightarrow 1$ transitions of SiO and CS, the $J_k = 3_k \rightarrow 2_k$ and $J_k = 2_k \rightarrow 1_k$ transitions of CH_3OH, and the $J = 1 \rightarrow 0$ transition of HCO^+, made with Swedish-ESO Submillimetre Telescope (SEST), toward the highly collimated bipolar outflow BHR 71. Broad wing emission was detected toward the outflow lobes in all the observed molecular lines. The shapes of the profiles are strikingly different from molecule to molecule. For CS and HCO^+ the emission from the outflowing gas appears as a weak broad feature superposed upon a strong narrow emission from the quiescent ambient gas. For CH_3OH the intensity of the broad emission feature is considerably stronger than that of the narrow component, whereas for SiO the broad feature completely dominates the emission spectra. The spatial distribution of the integrated wing emission is considerably extended and broadly similar in all the observed molecular transitions, showing well-separated blueshifted and redshifted lobes with FWHM angular sizes of $2'.4 \times 1'.3$ and $2'.4 \times 1'.4$, respectively. We find that the abundance of methanol and silicon monoxide in the outflow lobes is enhanced with respect to that of the ambient cloud by factors of up to ~ 40 and 350, respectively. The large enhancements of methanol and silicon monoxide in the outflow lobes are most likely due to the release from grains of ice mantles and Si-bearing species via shocks produced by the interaction between the outflow and dense ambient gas. On the other hand, we find that the abundance of HCO^+ in the outflowing gas is smaller than that in the ambient gas by about a factor of 20, a decrease consistent with theoretical predictions of shock models.

Subject headings: ISM: abundances — ISM: individual (BHR 71) — ISM: jets and outflows — ISM: molecules

1. INTRODUCTION

BHR 71 (Bourke, Hyland, & Robinson 1995a; Bourke et al. 1995b) or Sandqvist 136 (Sandqvist 1977) is a well-isolated Bok globule, located at a distance of ~ 200 pc from the Sun, which harbors a highly collimated bipolar outflow near its center (Bourke et al. 1997; hereafter Paper I; see Fig. 1). The CO outflow is found to be well described as a biconical flow, with a semiopening angle of 15° and inclined from the line of sight by an angle of $\sim 84°$, in which the gas moves outward with a constant radial velocity (with respect to the cone apex) of ~ 28 km s^{-1}. The outflow appears to be driven by a very young stellar object, with a total luminosity of $\sim 9\ L_\odot$, possibly still undergoing accretion of matter. Its characteristics at infrared and millimeter wavelengths are similar to those of the class 0 objects (André 1995).

The class of highly collimated outflows is thought to be driven by jets that accelerate the ambient gas through the propagation of shocks (e.g., Raga & Cabrit 1993). The interaction of high-velocity jets from young stars with the surrounding ambient gas generates strong shock waves that are expected to produce a significant transformation of the physical properties of the molecular surroundings, as well as of its chemical composition (see review by Bachiller 1996). Although there has been a substantial amount of work on the physical characteristics of outflows, very little is known about their chemical composition. Very few multiline mapping studies of molecular outflows have been performed so far (Blake et al. 1995; Bachiller & Pérez Gutiérrez 1997). Basic questions such as (1) How is the chemistry of the swept-up ambient molecular material affected by the winds from young stellar objects? and (2) Do molecular abundances serve as sensitive probes of the evolutionary stage of bipolar outflows? (e.g., van Dishoeck & Blake 1995) have not yet been answered. The lobes of the BHR 71 outflow extend by $\sim 4'$ in the plane of the sky, which makes it an ideal source for a detailed study, using single-dish instruments, of the physical and chemical characteristics across highly collimated, low-velocity shocks. In this article we report on extensive molecular observations, made with the Swedish-ESO Submillimetre Telescope (SEST), of the BHR 71 outflow in rotational transitions of silicon monoxide (SiO), methanol (CH_3OH), carbon monosulfide (CS), and the formyl ion (HCO^+).

[1] AAO/ATNF Postdoctoral Fellow. Present address: Anglo-Australian Observatory, P.O. Box 296, Epping, NSW 2121, Australia; tlb@aaoepp.aao.gov.au.

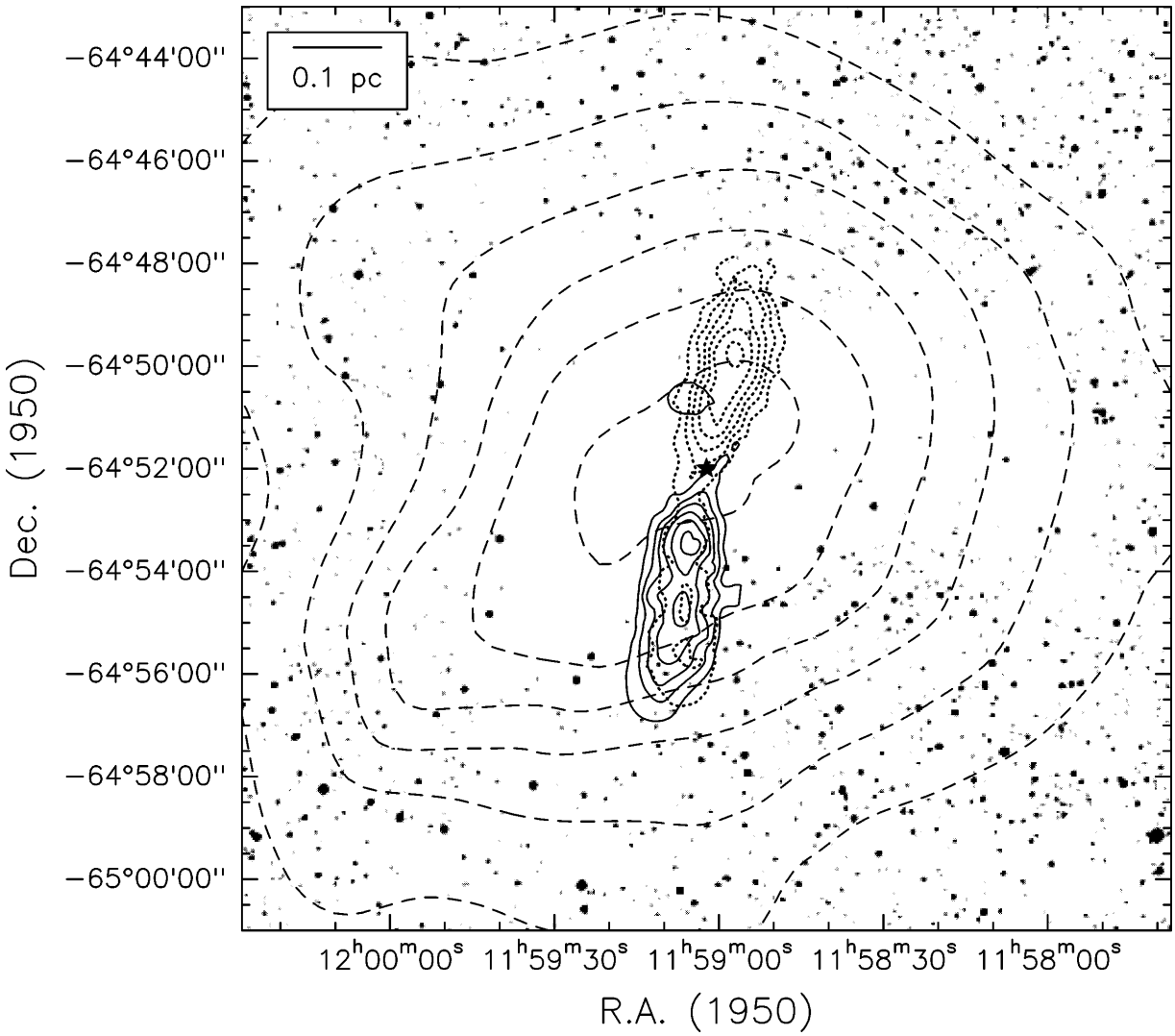

FIG. 1.—Contour map of velocity-integrated CO $J = 1 \rightarrow 0$ line wing emission from the BHR 71 bipolar outflow, superposed on a V-band image of the globule taken from the Digitized Sky Survey. Solid contours correspond to the emission integrated in the velocity range from -14 to -6 km s^{-1} (*blueshifted wing*) and short-dashed contours to the integrated emission in the velocity range from -3 to 7 km s^{-1} (*redshifted wing*). Contours are 20%, 35%, 50%, 65%, 80%, and 95% of the peak $\int T_A^* \, dv$ of 25.8 K km s^{-1} in the blue lobe and 31.7 K km s^{-1} in the red lobe. Long-dashed contours represent ^{13}CO $J = 1 \rightarrow 0$ emission integrated between -6 and -3 km s^{-1}. Contours for ^{13}CO are 20%, 35%, 50%, 65%, 80%, and 95% of the peak of $\int T_{mb} \, dv$ of 2.8 K km s^{-1}. The star marks the position of the millimeter-*IRAS* source 11590−6452 (Paper I). The ^{12}CO data are from SEST and the ^{13}CO data from the CTIO radio telescope (Paper I).

2. OBSERVATIONS

The observations were carried out using the 15 m SEST located on La Silla, Chile, during 1995 September and October. The molecules, transitions, and frequencies observed and the instrumental parameters are summarized in Table 1. The antenna half-power beamwidth and main beam efficiency of the telescope at the different observed frequencies are given in columns (4) and (5) of Table 1, respectively. We used SiS receivers to simultaneously observe the 2 and 3 mm lines of silicon monoxide, methanol, and carbon monosulfide. Single-sideband receiver temperatures were typically 120 K for both receivers. As back end we used high-resolution acousto-optical spectrometers providing a channel separation of 43 kHz and a total bandwidth of 43 MHz. The resulting spectral resolutions are given in column (6) of Table 1. Within the available bandwidth, three rotational lines of CH_3OH could be observed at 2 mm ($J_k = 3_0 \rightarrow 2_0$ A$^+$, $J_k = 3_{-1} \rightarrow 2_{-1}$ E, and $J_k = 3_0 \rightarrow 2_0$ E lines) and four rotational lines at 3 mm ($J_k = 2_1 \rightarrow 1_1$ E, $J_k = 2_0 \rightarrow 1_0$ E, $J_k = 2_0 \rightarrow 1_0$ A$^+$, and $J_k = 2_{-1} \rightarrow 1_{-1}$ E lines).

During the 1995 September observing session we mapped the molecular emission within a region of $\sim 5' \times 10'$, with 1′ spacings, in each of the above transitions. The observations were performed in the position switched mode, with the OFF position located at $\alpha_{1950} = 11^h53^m44^s.7$, $\delta_{1950} = -65°13'58''$. The integration times on source were typically 3 minutes per position. The resulting rms noise in antenna temperature is given in column (7) of Table 1. During the 1995 October observing run we undertook deeper observations toward the southeast 1 and northwest CO peaks in the outflow lobes (Paper I) and toward the center of the globule. The goal was to obtain sensitive data in order to perform rotational diagram analysis. The observed positions are at offsets from the *IRAS* source position ($\alpha_{1950} = 11^h59^m03^s.1$, $\delta_{1950} = -64°52'11''$) of (40″, −100″; SE1 peak), (−40″, 140″; NW peak), and (0″, 0″). We made five-point cross maps about each of these three positions, with

TABLE 1

OBSERVATIONAL PARAMETERS

Molecule (1)	Transition (2)	Frequency (MHz) (3)	Beam Size (FWHM arcsec) (4)	η (5)	Δv (km s^{-1}) (6)	Noise[a] (K) (7)
CH_3OH	$J_k = 2_0 \rightarrow 1_0$ A$^+$	96,741.42	52	0.73	0.133	0.06
	$J_k = 3_0 \rightarrow 2_0$ A$^+$	145,103.23	34	0.66	0.089	0.10
SiO	$J = 2 \rightarrow 1$	86,846.998	57	0.75	0.149	0.03
	$J = 3 \rightarrow 2$	130,268.702	40	0.68	0.099	0.04
CS	$J = 2 \rightarrow 1$	97,980.968	52	0.73	0.132	0.04
	$J = 3 \rightarrow 2$	146,969.049	34	0.66	0.088	0.06
	$J = 5 \rightarrow 4$	244,935.606	22	0.45	0.053	0.09
HCO^+	$J = 1 \rightarrow 0$	89,188.518	56	0.75	0.145	0.08
$H^{13}CO^+$	$J = 1 \rightarrow 0$	86,754.294	57	0.75	0.149	0.03

[a] 1 σ rms noise in antenna temperature.

15″ spacings, in the $J = 3 \rightarrow 2$ and $J = 2 \rightarrow 1$ lines of SiO and CS, and the $J_k = 3_k \rightarrow 2_k$ and $J_k = 2_k \rightarrow 1_k$ lines of CH_3OH. The integration time per position ranged between 4 and 8 minutes. The observations were performed in dual beam-switching mode, with a beam separation of 11′47″ in azimuth.

In addition, we supplement the above with observations of the $H^{13}CO^+$ $J = 1 \rightarrow 0$ and CS $J = 5 \rightarrow 4$ lines at the *IRAS* position that were undertaken in 1994 April. Details are given in Table 1.

3. RESULTS

The spectra of the emission in the seven observed molecular transitions, across the 5′ × 10′ region mapped with SEST with 1′ spacing, are shown in Figure 2. Also shown for comparison are the spectra of the ^{12}CO $J = 1 \rightarrow 0$ emission, taken from Paper I. Offsets are from the reference position at $\alpha_{1950} = 11^h59^m01^s.18$, $\delta_{1950} = -64°52'00''$, which itself is offset by $(\Delta\alpha, \Delta\delta) = (7'', 1'')$ from the position of the millimeter source as given in Paper I (note that the reference position quoted in Table 5 of Paper I is incorrect; the correct position is the one listed above). Two emission components, originating from physically and chemically different environments, can be distinguished from this figure. A narrow line emission component, at a velocity of -4.45 km s^{-1}, arising from the quiescent gas of the BHR 71 globule, and a broad line emission component that arises from the bipolar outflowing gas (cf. Paper I). The line wing emission was detected in all the observed molecular transitions. The shapes of the profiles are, however, different from molecule to molecule depending on the relative intensities between the narrow and broad components. Particularly striking are the cases of methanol and silicon monoxide molecules, for which the emission from the broad component is much stronger than that from the narrow component. The broad emission is detected at redshifted velocities with respect to the systemic ambient cloud velocity toward the northwest region of the map (the red lobe) and at blueshifted velocities toward the southeast region (the blue lobe).

To illustrate in more detail the differences between the line profiles, we show in Figure 3 the spectra of the line emission averaged across the blue lobe, red lobe, and central core region. Emission in the lines of SiO is detected only from the lobes, no (or very weak) emission is detected at the core of the globule at the level of 0.06 K. The CH_3OH profiles show broad, strong emission toward the lobes and narrow, weak emission at the velocity of the ambient cloud toward the core. The vertical bars shown in the spectra of methanol indicate the expected positions of the three rotational transitions within the displayed velocity range for a rest velocity of -4.45 km s^{-1}. On the other hand, the CS and HCO^+ profiles show a mixture of strong emission from the quiescent ambient cloud and relatively weaker wing emission at the position of the lobes. Figure 3 also shows that the average emission from the red lobe is brighter than that from the blue lobe, by roughly a factor of 2, and that toward the red lobe the wing emission in the SiO lines is considerably broader than in the CH_3OH lines. As discussed in Paper I the blue lobe appears to be breaking through the near side of the globule, resulting in a well-defined cavity being visible at optical wavelengths (Fig. 13 of Paper I). It is therefore likely that the amount of ambient material interacting with the outflow in the blue lobe is significantly less than in the red lobe, resulting in weaker emission being observed toward the blue lobe.

Maps of the velocity-integrated emission in the ranges of the blue wing (-9.1 to -5.5 km s^{-1}; *continuous line*) and red wing (-3.1 to 0.5 km s^{-1}; *dashed line*) are shown in Figure 4. The star marks the position of the millimeter continuum source. Also shown, for comparison, is a map of the ^{12}CO $J = 1 \rightarrow 0$ emission in the same velocity range. The spatial distribution of the integrated wing emission is broadly similar in all the observed molecular transitions, showing well-separated blueshifted and redshifted lobes aligned in a direction with a position angle of $\sim 168°$. From the maps of the SiO, CH_3OH, and CS emission we measure FWHM angular sizes of 2′.4 × 1′.3 for the red lobe and 2′.4 × 1′.4 for the blue lobe. The peaks of the molecular emission are offset by $\sim 2'$ (~ 0.1 pc) from the central millimeter-source. Although the integrated wing emission morphology is notably similar in the 2 and 3 mm transitions of a given molecule, there are some differences in the spatial distribution of different molecular species. Compared to methanol and CS, the SiO lobes appear to extend further away from the driving source, exhibiting spatial extensions similar to those of the CO lobes. Whereas some of the differences in the position of the peak emission seen in Figure 4 can be ascribed to our spatial undersampling, this circumstance cannot explain the differences in spatial extent that appear to be intrinsic to the data. With the present observations is not possible to discern whether the emission from the lobes arises from either a uniform distribution of high-velocity gas or from small cloudlets. The low values of the observed main beam brightness temperature suggest, however, that clumpiness is important.

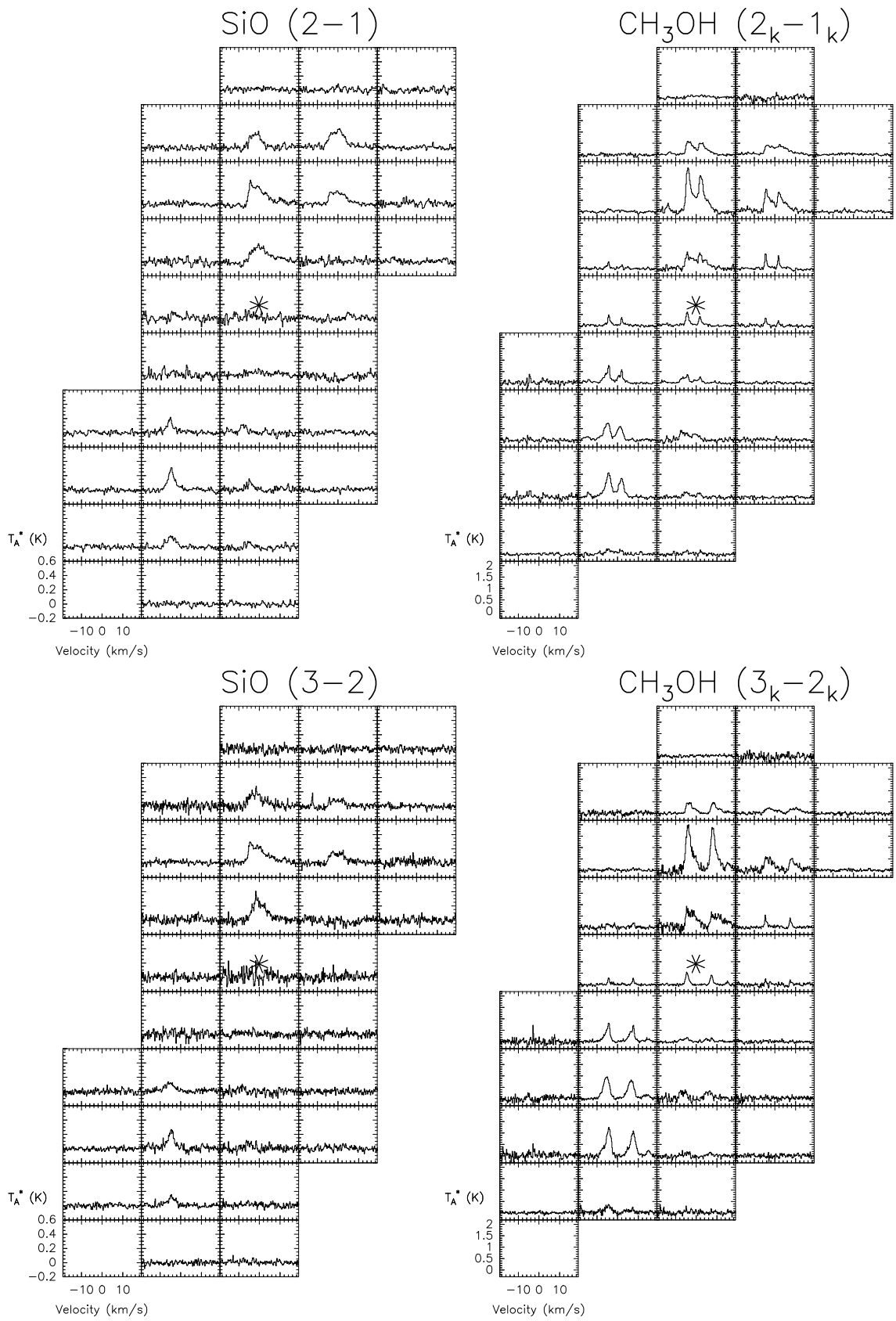

FIG. 2.—Observed spectra of several molecules across the central 5′ × 10′ of the BHR 71 globule. The grid spacing is 1′. The asterisk marks the position of the millimeter-*IRAS* source 11590−6452 (Paper I). In each box the velocity scale ranges from −19 to 19 km s^{-1}. The antenna temperature scale is from −0.2 to 0.6 K for SiO, −0.3 to 2.2 K for CH_3OH, −0.2 to 1.0 K for CS, −0.3 to 3.0 K for HCO^+, and −1.0 to 10.0 K for CO. The coordinates of the central position (asterisk) are $\alpha_{1950} = 11^h59^m01^s.18$, $\delta_{1950} = -64°52'00''$. North is at the top; east is to the left.

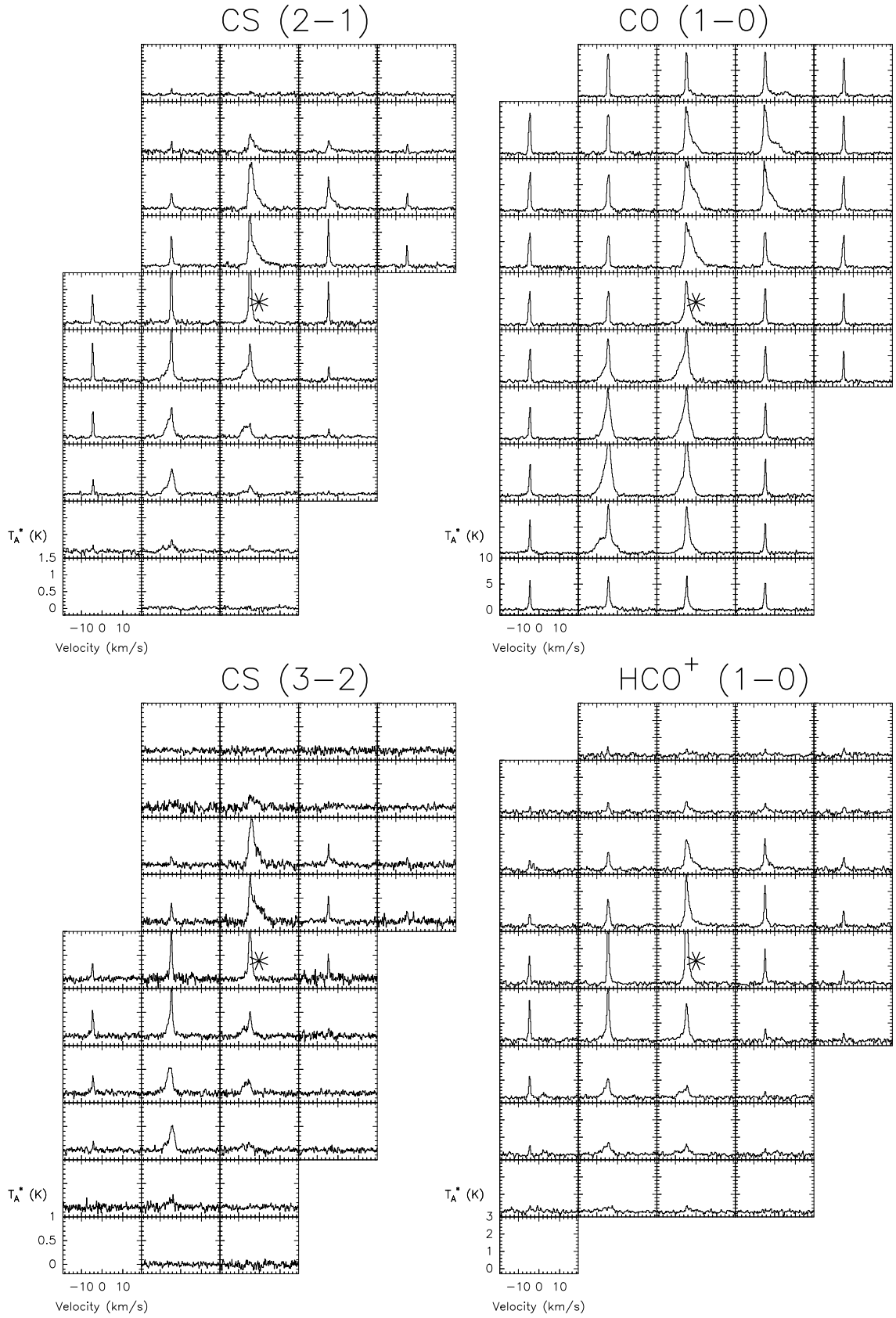

FIG. 2.—*Continued*

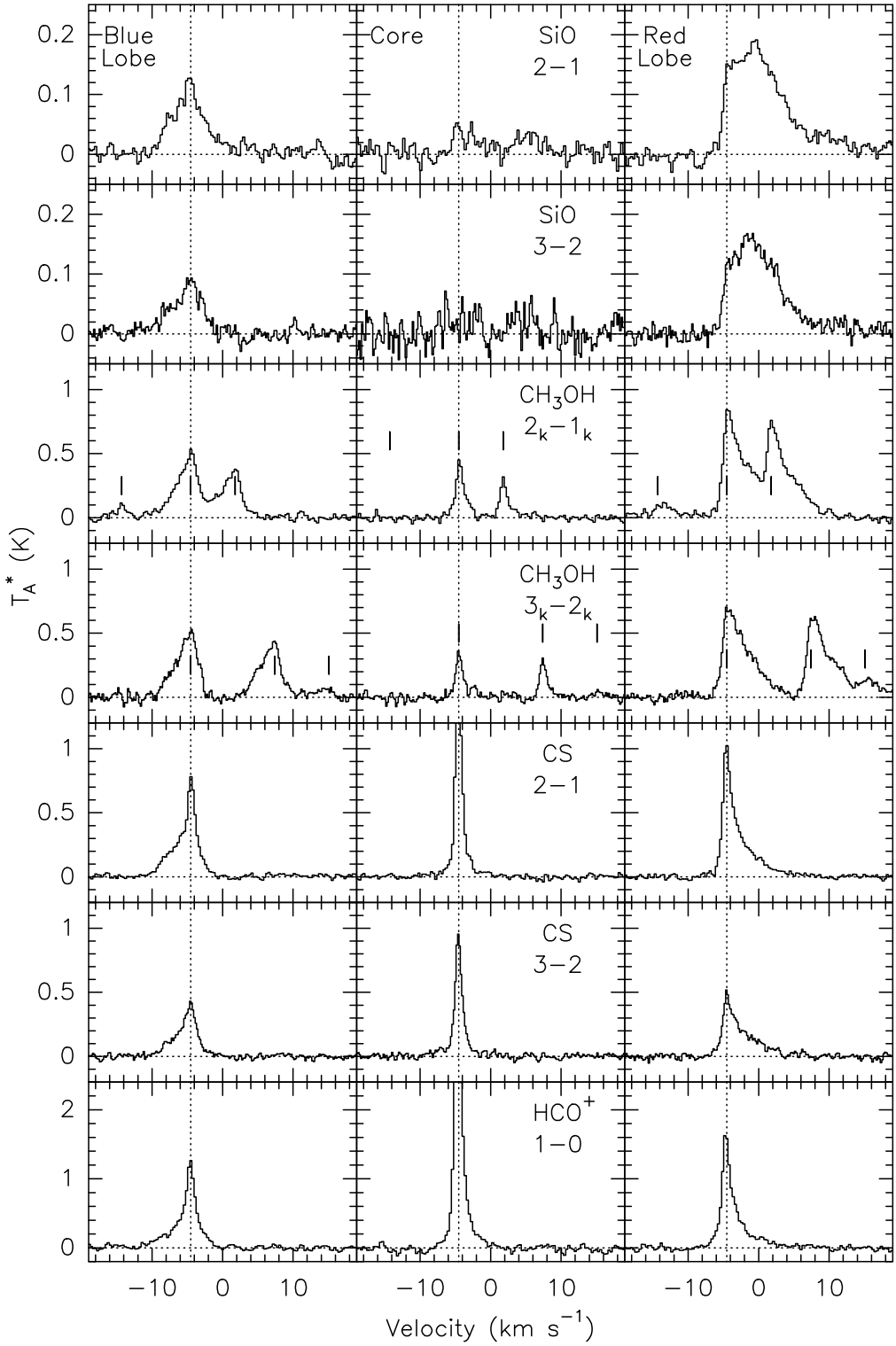

FIG. 3.—Spectra of the spatially integrated line emission from the blue (*left column*) and red (*right column*) lobes of the BHR 71 outflow and from the "core" region (centered on IRAS 11590−6452; *middle column*). The observed transitions are labeled in the upper right corner of the spectra shown in the middle column. The vertical dashed line indicates the systemic velocity of the globule of -4.45 km s^{-1}. The vertical ticks on the CH_3OH spectra indicate the different CH_3OH transitions observed.

The spectra of the emission in the lines of methanol, silicon monoxide, and carbon monosulfide toward the SE1, NW and core positions obtained from the pointed, higher signal-to-noise (S/N) observations are shown in Figure 5. In these deep integrations weak SiO emission from the core position, barely evident in the shorter integrations shown in Figure 3, is clearly seen. The shape of the methanol lines toward the SE1 and NW peaks are distinctly different. Although the profile of the emission in each individual line of methanol from the SE1 peak can be well fitted by a single

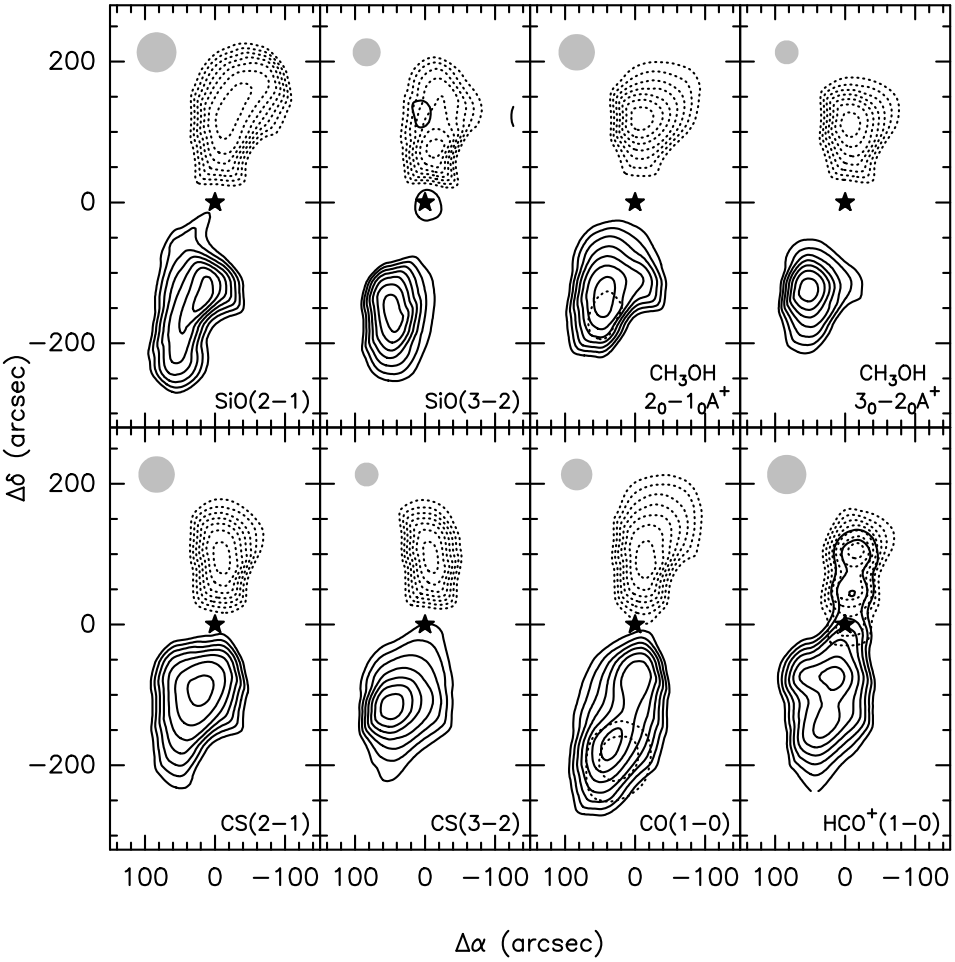

FIG. 4.—Contour maps of velocity-integrated line wing emission from the BHR 71 bipolar outflow. Continuous contours correspond to the emission integrated in the velocity range from -9.1 to -5.5 km s^{-1} (*blueshifted wing*) and dashed contours to the integrated emission in the velocity range from -3.1 to 0.5 km s^{-1} (*redshifted wing*). Contours are 35%, 45%, 55%, 65%, 75%, 85%, and 95% of the peak $\int T_A^* \, dv$ in each lobe. The peaks are 0.37 K km s^{-1} for the blue lobe and 0.88 K km s^{-1} for the red lobe of the SiO $J = 2 \rightarrow 1$ map, 0.32 (*blue*) and 1.01 (*red*) K km s^{-1} for the SiO $J = 3 \rightarrow 2$ map, 1.22 and 2.83 K km s^{-1} for the CH_3OH $J_k = 2_0 \rightarrow 1_0$ map, 1.78 and 2.81 K km s^{-1} for the CH_3OH $J_k = 3_0 \rightarrow 2_0$ map, 1.19 and 1.85 K km s^{-1} for the CS $J = 2 \rightarrow 1$ map, 0.85 and 1.47 K km s^{-1} for the CS $J = 3 \rightarrow 2$ map, 15.71 and 17.08 K km s^{-1} for the CO $J = 1 \rightarrow 0$ map, and 1.48 and 2.14 K km s^{-1} for the HCO^+ map. The star indicates the position of the millimeter-*IRAS* source 11590−6452. The beam FWHM for each transition is indicated in the upper left of each map by the shaded circle. Offsets are relative to $\alpha_{1950} = 11^h59^m01^s.18$, $\delta_{1950} = -64°52'00''$.

Gaussian component, those toward the NW peak are clearly non-Gaussian; their shapes are better reproduced by a blend of emission from a narrow component and a broader redshifted component. In Table 2 we summarize the results of Gaussian profiles fit to the emission from the SE1 peak (one Gaussian component per line), NW peak (two Gaussian components per line), and core position (one Gaussian component per line). The center velocities V_{rel} given in this table are velocities relative to the ambient cloud velocity ($V_{rel} = V - V_0$, where $V_0 = -4.45$ km s^{-1}). The six methanol lines observed toward the SE1 peak have an average relative center velocity of -1.3 km s^{-1} and an average width of 3.7 km s^{-1}. On the other hand, the two Gaussian components fitting the methanol emission from the NW peak have average relative center velocities of 0.3 and 3.0 km s^{-1} and average widths of 2.0 and 3.8 km s^{-1}, respectively. Hereafter we will refer to these components as the low (LV) and intermediate (IV) redshifted flow velocity components. Even though the LV emission from the NW peak has a center velocity similar to the systemic cloud velocity ($V_{rel} = 0.3$ km s^{-1}), it is unlikely that it arises from the cold, quiescent ambient gas (see § 5.1). The lines of methanol emission from the core region have an average relative center velocity of 0.1 km s^{-1} and an average width of 1.8 km s^{-1} and presumably trace high-density ambient gas at the center of the BHR 71 globule. Toward the core position we also detect relatively strong emission at $V_{rel} \sim 28.1$ km s^{-1}, corresponding to emission from the $J_k = 3_{12} \rightarrow 2_{21}$ rotational line of C_3H_2 (Vrtilek, Gottlieb, & Thaddeus 1987). Emission from this transition is not detected toward the lobes of the outflow, suggesting that this line might be a good probe for studies of the kinematics and physical conditions of the molecular gas surrounding the central energy source.

The peak intensity, relative center velocity, width, and integrated intensity of the SiO emission from the NW peak, SE1 peak, and core region, obtained from Gaussian fits to the profiles shown in Figure 5, are given in Table 3. As noted before, owing to the higher sensitivity, SiO emission is detected toward the core position. The line center velocity is, however, displaced by ~ 1.5 km s^{-1} from the ambient cloud velocity, suggesting that the SiO emission seen

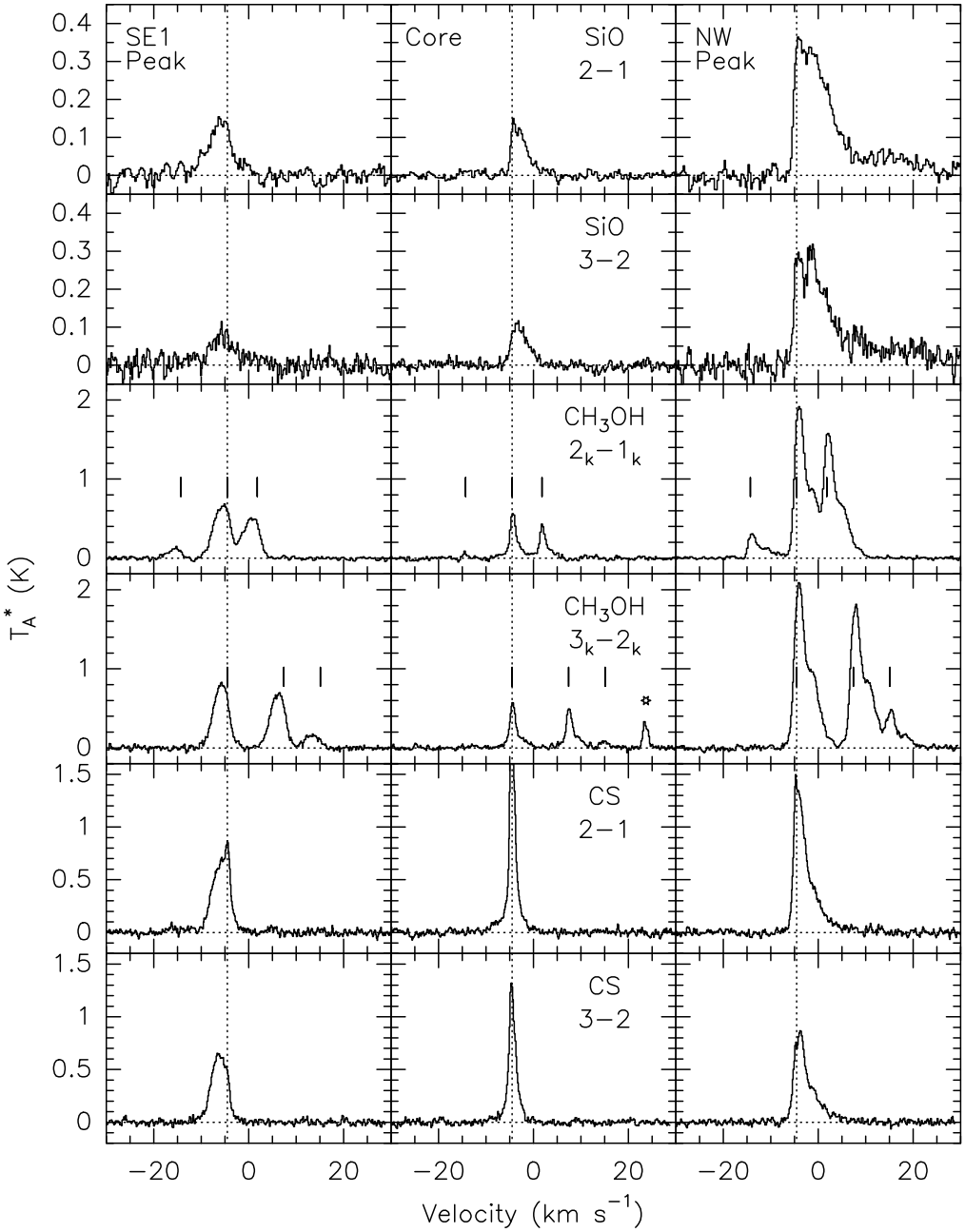

FIG. 5.—Spectra of the line emission observed toward the SE1 peak (offset 20″, −80″ from the millimeter-*IRAS* source) of the blue lobe (*left column*), toward the millimeter source (the "core" position, *middle column*), and toward the NW peak (offset −40″, 140″) of the red lobe (*right column*), as defined in Paper I. Transitions are labeled in the upper right corner of the spectra shown in the middle column. The velocity scale is from −29 to 29 km s^{-1}. The vertical dashed line indicates the systemic velocity of the globule of −4.45 km s^{-1}. The vertical ticks on the CH_3OH spectra indicate the different CH_3OH transitions observed, and the star in the CH_3OH $J_k = 3_k \rightarrow 2_k$ panel indicates the $J_k = 3_{12} \rightarrow 2_{21}$ transition of C_3H_2.

toward the core does not arise solely from the quiescent ambient gas. The SiO line profiles observed toward the NW red peak exhibit, in addition to strong emission in the LV and IV ranges, weaker, more redshifted, emission up to radial velocities of ∼25 km s^{-1} from the ambient cloud radial velocity. We will refer to this feature as the high-velocity (HV) component. From the inclination angle i and the semiopening angle θ of a biconical outflow, it is possible to derive the actual flow velocity from the maximum observed radial velocity (Cabrit & Bertout 1990). Using $i = 84°$ and $\theta = 15°$ (Paper I), we find that the HV gas has a flow velocity of ∼70 km s^{-1}. However, the semiopening angle was determined using the observed LV and IV emission. It is generally found that the gas moving at the highest velocities is more collimated than the slower moving gas in molecular outflows (e.g., Bachiller et al. 1990; Paper I), and so the value of 70 km s^{-1} for the HV component is most likely only a lower limit to the true velocity. Emission from the HV component is neither evident in the other molecular species observed here, nor toward the SE1 peak of the blue lobe, although it is seen in deep CO observations toward the northeast peak (T. L. Bourke 1998, private communication). As shown in Table 3, three Gaussian components were required to fit the SiO profiles observed at the

TABLE 2

CH_3OH LINE PARAMETERS

Transition	V_{rel}[a] (km s^{-1})	Δv (km s^{-1})	T_a^* (K)	$\int T_a^*$ dv (K km s^{-1})	Comments[b]
Red Lobe: NW Peak					
$J_k = 2_0 \rightarrow 1_0$ E	0.2	1.9	0.30	0.60	LV
	3.2	3.5	0.14	0.51	IV
$J_k = 2_0 \rightarrow 1_0$ A$^+$	0.4	2.1	1.96	4.41	LV
	3.1	3.2	0.87	2.95	IV
$J_k = 2_{-1} \rightarrow 1_{-1}$ E.....	0.3	1.9	1.28	2.59	LV
	2.5	4.8	0.71	3.64	IV
$J_k = 3_0 \rightarrow 2_0$ A$^+$	0.3	2.0	1.73	3.77	LV
	2.8	4.4	0.96	4.46	IV
$J_k = 3_{-1} \rightarrow 2_{-1}$ E.....	0.3	2.1	1.59	3.57	LV
	3.0	4.0	0.81	3.44	IV
$J_k = 3_0 \rightarrow 2_0$ E	0.2	2.2	0.45	1.03	LV
	3.2	2.9	0.15	0.47	IV
Blue Lobe: SE1 Peak					
$J_k = 2_0 \rightarrow 1_0$ E	−1.4	3.4	0.12	0.43	LV and IV
$J_k = 2_0 \rightarrow 1_0$ A$^+$	−1.2	4.1	0.68	2.96	LV and IV
$J_k = 2_{-1} \rightarrow 1_{-1}$ E.....	−1.2	3.7	0.53	2.08	LV and IV
$J_k = 3_0 \rightarrow 2_0$ A$^+$	−1.4	3.7	0.83	3.26	LV and IV
$J_k = 3_{-1} \rightarrow 2_{-1}$ E.....	−1.3	3.6	0.71	2.69	LV and IV
$J_k = 3_0 \rightarrow 2_0$ E	−1.7	3.5	0.17	0.62	LV and IV
Core: Millimeter-Source					
$J_k = 2_0 \rightarrow 1_0$ E	−0.2	1.0	0.078	0.084	
$J_k = 2_0 \rightarrow 1_0$ A$^+$	0.2	1.8	0.53	1.03	
$J_k = 2_{-1} \rightarrow 1_{-1}$ E.....	0.2	1.9	0.37	0.76	
$J_k = 3_0 \rightarrow 2_0$ A$^+$	0.2	1.8	0.53	0.99	
$J_k = 3_{-1} \rightarrow 2_{-1}$ E.....	0.2	2.0	0.44	0.97	
$J_k = 3_0 \rightarrow 2_0$ E	−0.2	2.1	0.083	0.19	

[a] Velocity relative to the ambient cloud velocity of −4.45 km s^{-1}.

[b] LV indicates low-velocity component, IV indicates intermediate velocity component (see text).

NW peak position of the red lobe. Even though the solutions are formally correct and give similar line center velocities and line widths for both SiO transitions, the assumption of Gaussian profiles for the wing emission is arguable, and therefore these results should be taken only as illustrative.

4. ANALYSIS

4.1. *Column Densities and Rotational Temperatures*

In order to derive the rotational temperature T_{rot} and the total column density N_T of methanol, we used a rotational

TABLE 3

SiO LINE PARAMETERS

Transition	V_{rel}[a] (km s^{-1})	Δv (km s^{-1})	T_a^* (K)	$\int T_a^*$ dv (K km s^{-1})	Comments[b]
Red Lobe: NW Peak					
$J = 2 \rightarrow 1$.....	0.4	2.0	0.23	0.48	LV
	3.8	6.6	0.30	2.08	IV
	16.6	23.8	0.061	1.54	HV
$J = 3 \rightarrow 2$.....	0.3	2.1	0.20	0.46	LV
	3.8	5.6	0.24	1.44	IV
	15.1	20.5	0.051	1.11	HV
Blue Lobe: SE1 Peak					
$J = 2 \rightarrow 1$.....	−1.6	5.9	0.14	0.87	LV and IV
$J = 3 \rightarrow 2$.....	−1.0	5.0	0.071	0.37	LV and IV
Core: Millimeter-Source					
$J = 2 \rightarrow 1$.....	1.3	3.5	0.13	0.48	
$J = 3 \rightarrow 2$.....	1.6	4.1	0.10	0.45	

[a] Velocity relative to the ambient cloud velocity of −4.45 km s^{-1}.

[b] LV indicates low-velocity component, IV indicates intermediate velocity component, HV indicates high-velocity component (see text).

diagram analysis (see, e.g., Linke, Frerking, & Thaddeus 1978; Blake et al. 1987), with the assumptions of optically thin conditions and local thermodynamic equilibrium (LTE), which relates the integrated line intensity, rotational temperature, and column density via

$$\frac{3k \int T_{\rm mb}\, dv}{8\pi^3 \mu^2 \nu S} = \frac{N_u}{g_u} = \frac{N_T}{Q(T_{\rm rot})} \exp\left(-\frac{E_u}{kT_{\rm rot}}\right), \qquad (1)$$

where μ, ν, and S are the transition dipole moment, frequency, and line strength of the transition, respectively, $\int T_{\rm mb}\, dv$ is the velocity-integrated main beam brightness obtained directly from the observations, E_u is the upper state energy, and $Q(T_{\rm rot})$ is the rotational partition function. In Table 4 we summarize the rotational temperatures and column densities of CH_3OH derived toward selected positions of the red and blue lobes of the outflow. For the blue lobe we integrated the emission in the LSR velocity range from -9.3 to -5.3 km s^{-1}, whereas for the red lobe we integrated the emission in the LSR velocity range from -3.7 to 0.3 km s^{-1}. These ranges have been chosen such that there is neither overlap between the emission in the different components of the methanol lines nor a possible contribution from the ambient cloud gas. They mainly span the intermediate velocity range of the outflowing gas. As a mode of illustration, we show in Figure 6 the rotational diagrams corresponding to the CH_3OH emission from the SE1 and NW peaks of the blue and red lobes. Toward these positions we detected emission in seven rotational lines of CH_3OH. The rotational temperature and N_T/Q ratio of methanol derived from a linear least squares fit to these data are shown in the lower left corner. The rotational temperatures of the outflowing gas at the different positions are broadly similar, with an average value of 7 K and a dispersion of 1 K. A similar analysis was performed for the CS and SiO molecules for which we detected emission in two rotational lines. The results are summarized in Table 4. We find that there is no significant difference among the rotational temperatures derived using different molecular species.

The rotational diagram analysis cannot be applied to the outflow CO emission because the lines are optically thick (Paper I). However, the excitation temperature of CO can be estimated from the observed main beam brightness temperature when the line emission is optically thick and the filling factor of the emission is unity. At the NW peak position of the red lobe we find an average main beam ^{12}CO $J = 2 \rightarrow 1$ brightness temperature, in the range of velocities between -3 and -2 km s^{-1}, of 17 K. At the SE1 and SE2 peak positions of the blue lobe we measure average main beam ^{12}CO $J = 2 \rightarrow 1$ brightness temperatures, in the range of velocities between -7 and -6 km s^{-1}, of $\sim$13 K. We will adopt these values as the excitation temperatures of the outflowing CO gas in the red and blue lobes of BHR 71, respectively. We used the ^{12}CO $J = 2 \rightarrow 1$ data because they were collected using a smaller beam than the ^{12}CO $J = 1 \rightarrow 0$ data, thus minimizing a possible correction for a filling factor different from 1, and because the optical depth of the emission in the ^{12}CO $J = 2 \rightarrow 1$ line is larger than that in the ^{12}CO $J = 1 \rightarrow 0$ line.

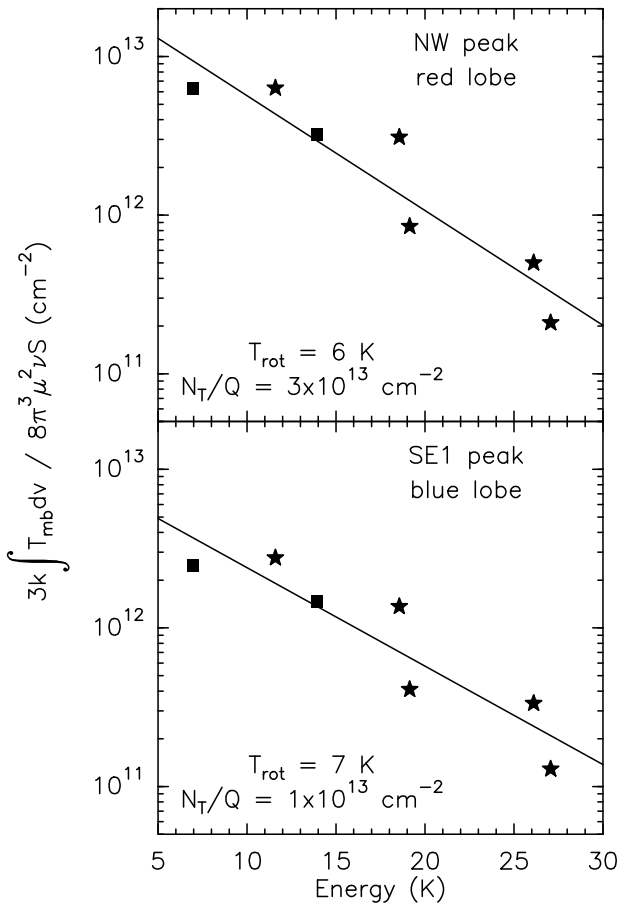

FIG. 6.—Rotational diagrams for the methanol transitions observed toward the red and blue lobes of BHR 71. The lines correspond to least squares linear fits to the observed data. The derived values of the rotational temperature and total column density are given in the lower left corner.

4.2. *Densities*

To determine the density in the outflow we used the CS $J = 2 \rightarrow 1$ and $J = 3 \rightarrow 2$ observations and a spherically

TABLE 4

DERIVED PARAMETERS OF OUTFLOWING GAS

Offset Position[a]	Lobe	CH_3OH T_R (K)	CH_3OH N_T/Q (cm^{-2})	CH_3OH N_T (cm^{-2})	SiO T_R (K)	SiO N_T/Q (cm^{-2})	SiO N_T (cm^{-2})	CS T_R (K)	CS N_T/Q (cm^{-2})	CS N_T (cm^{-2})	HCO^+ N_T (cm^{-2})	CO T_R (K)	CO N_T (cm^{-2})
(1, −3)	Blue	6	8.7×10^{12}	2.0×10^{14}	9	9.8×10^{10}	6.6×10^{11}	6	9.9×10^{11}	5.9×10^{12}	8.7×10^{11}	13	9.2×10^{16}
(1, −2)	Blue	9	6.1×10^{12}	1.4×10^{14}	9	8.1×10^{10}	5.4×10^{11}	8	8.4×10^{11}	5.0×10^{12}	9.7×10^{11}	13	2.5×10^{17}
SE1	Blue	7	1.0×10^{13}	2.3×10^{14}	6	2.6×10^{11}	1.8×10^{12}	10	1.2×10^{12}	6.9×10^{12}	...	...	...
(0, 2)	Red	6	2.2×10^{13}	5.0×10^{14}	8	2.9×10^{11}	2.0×10^{12}	7	1.9×10^{12}	1.1×10^{13}	1.9×10^{12}	17	3.5×10^{17}
(−1, 2).....	Red	6	1.6×10^{13}	3.6×10^{14}	6	2.4×10^{11}	1.6×10^{12}	6	1.8×10^{12}	1.1×10^{13}	8.3×10^{11}	17	1.8×10^{17}
NW	Red	6	3.2×10^{13}	7.2×10^{14}	7	4.6×10^{11}	3.1×10^{12}	7	2.2×10^{12}	1.3×10^{13}	...	...	...

[a] Offsets in arcminutes are relative to R.A.(1950) = $11^h59^m20^s.0$, decl.(1950) = $-64°51'00''$.

symmetric large velocity gradient (LVG) statistical equilibrium code (see, e.g., Snell et al. 1984; Mundy et al. 1986), which includes radiation trapping due to optical depth effects. Inputs of the code are the column density, determined in our case from the rotational diagram analysis, and the kinetic temperature of the gas. Since a direct estimate of the last is not available, we ran the model for kinetic temperatures of 15, 25, 50, and 100 K. The LVG analysis shows that the $J = 3 \rightarrow 2$ to $J = 2 \rightarrow 1$ intensity ratio is relatively insensitive to the kinetic temperature in this range, and that the gas density that produces the best fit to the observations, assuming the outflow CS emission is optically thin, is $n(H_2) \sim 10^5$ cm^{-3}.

A determination of the density of the ambient gas using the same procedure as above is probably not reliable, owing to the possibility that the CS line may be optically thick. To avoid this problem we made use of the observation of the $J = 5 \rightarrow 4$ line at the (0, 0) position, for which we have a 3 σ detection. By using three CS transitions optical depth effects are accounted for by the LVG analysis. We assume that the ambient gas temperature of the BHR 71 globule is $\sim$10–15 K, as derived by Bourke et al. (1995b) from observations of ammonia lines. The intensities and line widths of the three CS transitions are solved for simultaneously to give the column density and density, obtaining $N(\mathrm{CS}) \sim 2 \times 10^{13}$ cm^{-2} and $n(H_2) \sim 3 \times 10^5$ cm^{-3} for temperatures in the adopted range. For comparison, Bourke et al. (1995b) estimate $n(H_2) \sim 3 \times 10^4$ cm^{-3} from ammonia observations with a much larger beam. Observations of $C^{34}S$ are required to more accurately determine the density of the ambient gas.

4.3. *Temperatures*

As discussed in § 4.1, we find that the rotational temperature of the methanol emission from the outflowing gas in BHR 71 is typically $\sim$7 K. Whether this temperature provides an estimate of the kinetic temperature of the outflowing gas is arguable due to the possibility that the methanol populations may be subthermally excited (Bachiller et al. 1995; Avery & Chiao 1996). For the L1157 outflow Bachiller et al. (1995) found that the rotational temperature of methanol is $\sim$12 K, whereas Tafalla & Bachiller (1995) determined, from ammonia observations, that the kinetic temperature of the outflowing gas is $\sim$100 K, indicating that the methanol populations in the outflowing gas of L1157 are extremely subthermal. To assess whether a similar situation exists in the BHR 71 outflow we undertook a methanol excitation analysis using the same statistical equilibrium LVG code as Bachiller et al. (1995). We include levels up to $J = 12$ and $K = 3$, with the maximum number of levels set to 100. For the calculations we assume $N/\Delta v = 1 \times 10^{14}$ cm^{-2} (km s^{-1})$^{-1}$ in the outflow, which is consistent with our data, and ran the model for a density of 10^5 cm^{-3} and kinetic temperatures of 12, 50, and 100 K. Our aim here is not to determine precisely the kinetic temperature, which is not feasible considering the limited number of data points and the complexities of the methanol molecule, but to estimate the range of kinetic temperatures that is consistent with our data. In particular, when the methanol is subthermally excited model rotational diagrams including a large number of transitions show that excitation temperatures of transitions along k-ladders are larger than for transitions between k-ladders (Bachiller et al. 1995), with the result that the derived T_{rot} is very dependent on the transitions included in the analysis. From the analysis we find that our methanol observations are consistent with $T_K \sim$ 50–100 K in the outflow, suggesting that the methanol is highly subthermally excited.

4.4. *Molecular Abundances*

The chemical composition of a gas cloud is usually characterized by the fractional abundance of molecules relative to molecular hydrogen, the main constituent of the interstellar gas. The abundance of H_2 in the lobes of the BHR 71 outflow is not known and is difficult to estimate. Therefore, in the following discussion we will consider fractional abundances relative to the CO abundance that can be directly derived from our observations. We note that the $[\mathrm{CO}]/[H_2]$ abundance ratio seems to be rather insensitive to differences in physical conditions and chemistry in different molecular environments, having values in the range from 7×10^{-5} to 1×10^{-4}, a variation of only $\sim$40% (van Dishoeck et al. 1993). This variation could be explained by observations that indicate that up to 40% of the CO in dense clouds may be depleted onto grains (e.g., Whittet et al. 1989; Chiar et al. 1995). Some of this CO may be liberated in outflows by shocks, and so any comparison with CO that assumes a constant CO abundance may overestimate the relative abundance of other molecules. However, shock models predict that the abundance of CO remains relatively constant through the shock, whether J- or C-type (Iglesias & Silk 1978; Bergin, Melnick, & Neufeld 1998), and so this may not be a problem, although these models do not appear to consider the possibility of direct desorption of CO from grains.

The abundances of molecular species X relative to CO, [X]/[CO], in the outflowing gas of the BHR 71 lobes are given in Table 5. They were computed as the ratio of the molecular column density of species X, obtained from the rotational analysis (see Table 4), and the column density of CO molecules in the corresponding velocity range. The latter was computed from the ratio of the observed emission in the ^{12}CO and ^{13}CO lines assuming a ^{12}CO/^{13}CO ratio of 89 and an excitation temperature of 13 K for the blue lobe and 17 K for the red lobe (see Paper I for a description of the method). Since for the BHR 71 cloud the ambient gas and shocked gas are well distinguished, both spatially and kinematically, the derived abundances of the outflowing gas are not affected by the emission of the quiescent gas. We find that the $[CH_3OH]/[\mathrm{CO}]$ and $[\mathrm{SiO}]/[\mathrm{CO}]$ abundances toward the lobes are typically $\sim 1 \times 10^{-3}$ and $\sim 6 \times 10^{-6}$, respectively. The column densities of HCO^+ in the outflow were estimated from the observed emission in the $J = 1 \rightarrow 0$ line, assuming it is optically thin, and using the same excitation temperatures as for CO.

To quantitatively assess the chemical changes of the ambient medium due to the outflow phenomena requires a knowledge of the chemical abundances of the quiescent ambient gas. Since molecular observations of the BHR 71 globule away from the outflow system are not available, we will adopt as ambient gas abundances, where appropriate, those determined from our observations at the core position. The derived relative abundance of molecules in the ambient gas are presented in Table 5. The CO column density was determined, as described above, using the observations of the CO ($J = 1 \rightarrow 0$) and ^{13}CO ($J = 1 \rightarrow 0$) line emission assuming an excitation temperature of 11 K (Paper I). This method was also used to derive the HCO^+

TABLE 5

MOLECULAR ABUNDANCES RELATIVE TO CO

Feature	Offset Position[a]	[CH_3OH/CO]	[SiO/CO]	[CS/CO]	[HCO^+/CO]
BHR 71 Outflow					
Blue lobe.....	(1, −3)	2×10^{-3}	7×10^{-6}	6×10^{-5}	9×10^{-6}
Blue lobe.....	(1, −2)	6×10^{-4}	2×10^{-6}	2×10^{-5}	4×10^{-6}
Red lobe	(0, 2)	1×10^{-3}	6×10^{-6}	3×10^{-5}	5×10^{-6}
Red lobe	(−1, 2)	2×10^{-3}	9×10^{-6}	6×10^{-5}	5×10^{-6}
BHR 71 Ambient					
Core	(0, 0)	5×10^{-5}	...	8×10^{-6}	9×10^{-5}
Dark Clouds					
TMC-1	...	3×10^{-5}	$<3 \times 10^{-8}$	1×10^{-4}	8×10^{-5}
L134N	...	4×10^{-5}	$<5 \times 10^{-8}$	9×10^{-6}	1×10^{-4}

[a] Offsets are in arcminutes relative to $\alpha_{1950} = 11^h59^m01^s.18$, $\delta_{1950} = -64°52'00''$.

column density from observations of the HCO^+ ($J = 1 \rightarrow 0$) and $H^{13}CO^+$ ($J = 1 \rightarrow 0$) line emission. We find that the emission in the $J = 1 \rightarrow 0$ line of both CO and HCO^+ is optically thick. For CS and CH_3OH we used the rotational diagram method described in § 4.1, with the caveat that the CS $J = 2 \rightarrow 1$ lines may be optically thick, in which case the CS column density would be underestimated. However, the result is in good agreement with the value obtained from the LVG analysis of § 4.2. As a check we computed the relative abundance of CS at the (2′, −2′) offset position, which is away from the influence of the outflow and embedded source, and for which we have the ^{13}CO observations needed to determine the CO column densities. We find that the relative abundance of CS in this position is the same, within the errors, as the one derived toward the core. Also to assess a possible contribution to the CH_3OH core emission from the outflow, and/or a circumstellar disk, we computed the CO and CH_3OH column densities at the (1′, 0′) offset position, obtaining the same CH_3OH relative abundance. Since it may be argued that the emission observed toward the core position may not serve as a good probe of the chemical state of the ambient medium, we also show in Table 5 the relative abundances derived toward two starless low-mass dark clouds, the TMC-1 ridge and L134N (see van Dishoeck et al. 1993, and references therein). The abundances derived toward the core of BHR 71 are almost identical to those measured for L134N. Finally, we note that the BHR 71 ambient gas SiO abundance cannot be estimated from the observations at the core position since in this case the emission most likely originates from gas associated with the outflow process. In fact, SiO emission from quiescent gas is usually not detected. In particular, for TMC-1 and L134N only upper limits exist in the abundance of SiO. In the following discussion we adopt as fiducial value of the [SiO/CO] abundance ratio in the quiescent ambient gas a value of 4×10^{-8}, corresponding to the geometrical mean of the upper limits determined for the TMC-1 ridge and L134N cloud.

TABLE 6

ABUNDANCE ENHANCEMENT

	Blue Lobe		Red Lobe	
Molecule	(1, −3)	(1, −2)	(0, 2)	(−1, 2)
CH_3OH.....	40	10	30	40
SiO	290	90	220	350
CS	8	3	4	8
HCO^+	0.10	0.04	0.06	0.06

Table 6 gives the abundance enhancement factor of gas-phase molecular species in the BHR 71 outflow with respect to the ambient gas values in BHR 71. At the peak position of the red lobe the [CH_3OH]/[CO] and [SiO]/[CO] abundance ratios are enhanced with respect to that of the quiescent ambient gas in dark globules by factors of ~ 40 and ≥ 350, respectively. On the other hand, the abundances of HCO^+ at the peak of the lobes are smaller than that in the ambient gas by a factor of ~ 20.

5. DISCUSSION

The data presented in the previous section clearly illustrate that the chemistry of the molecular gas near the core of the globule has been substantially modified as a result of the interaction between the outflow and the ambient medium. The spectacular abundance enhancement in the lobes with respect to that of the ambient medium may be interpreted to indicate that shocks play an essential role in the production of these molecules (Bachiller 1996; Schilke et al. 1997; Caselli, Hartquist, & Havnes 1997). Shocks can raise the gas temperature and drive many chemical reactions that are inefficient at ambient cloud temperatures. They can also partially destroy dust grains leading to the injection of several absorbed atoms and molecules from the grain surface into the gas phase. In the following discussion we first compare the spatial distribution and line profile shape of the SiO emission from BHR 71 with those observed toward other outflows, which should provide clues about the type of shocks that give rise to the abundance enhancement in BHR 71. Then we discuss possible explanations for the enhancement or depletion in the abundance of each of the observed molecular species.

5.1. *Comparison with Other Outflows*

Strong abundance enhancement in SiO and/or CH_3OH have been detected in a number of other outflows, such as L1448 (Bachiller, Martín-Pintado, & Fuente 1991), IRAS 03282+3025 (Bachiller et al. 1994), and L1157 (Mikami et al. 1992; Bachiller et al. 1995; Zhang et al. 1995; Avery & Chiao 1996). The first two sources are representative of the class of bipolar outflows associated with supersonic jets. The L1448 CO outflow is characterized by the presence of an extremely high-velocity (EHV) outflow, at a velocity of ~ 65 km s^{-1} with respect to the ambient cloud velocity, and

a more standard high-velocity (SHV) outflow at a velocity of ~ 15 km s^{-1}. In this source the SiO emission is associated with high-velocity molecular bullets (Bachiller et al. 1991), probably tracing shocks produced by a central jet. The SiO line profiles observed toward the central region of L1448 exhibit two strong emission features blueshifted and redshifted from the ambient cloud velocity by about the velocity of the EHV flow. The blueshifted (redshifted) feature shows a steep decrease in intensity toward the blue (red) and a slower decline toward the ambient cloud velocity. Away from this position the SiO spectra show two velocity components of weaker emission associated with the EHV and the SHV outflows. In the case of IRAS 03282+3025, which also consists of a well-collimated jet of fast gas (at velocities of ~ 57 km s^{-1}) and a more extended, slower (at velocities of ~ 17 km s^{-1}) standard outflow component, the SiO emission is only detected at the end of the EHV blue lobe of the CO outflow (Bachiller et al. 1994), where possibly there is a maximum interaction of the outflow with the ambient gas. In the L1157 outflow the SiO emission toward the red CO lobe is located at the end of the lobe (Zhang et al. 1997), whereas toward the blue CO lobe is more widespread and appears as successive clumps that are interpreted as indicating the positions of bow shocks in the flow (Zhang et al. 1995). The SiO line profile observed toward the blue lobe shows a steep increase from the ambient cloud velocity toward the peak radial velocity and a gradual decrease toward the more blueshifted velocities. This line asymmetry is opposite to that exhibited by the blueshifted emission from the bullets of the L1448 flow.

The spatial distribution and spectral line shape of the SiO emission from the BHR 71 flow are similar to those of the L1157 outflow and markedly different from those of the other two sources, possible reflecting differences in the physical conditions of the ambient gas, driving source, and mechanism of shock excitation. The SiO line profile observed at the norhtwest position of the BHR 71 red lobe, showing a broad redshifted feature with a peak at a radial velocity close to the ambient cloud velocity, a gradual decrease in intensity from the peak toward more redshifted velocities, and a rapid decline toward the ambient cloud velocity, is very similar in shape (besides the reversal in velocity) to the line profile observed at the peak of the blue lobe of the L1157 outflow. These profiles, if produced by shocks, suggest that a small fraction of the molecular gas is accelerated to shock velocities, whereas the majority remain close to the ambient cloud velocity. For a shock moving with speed V_s, an observer that is at rest with respect to the preshock gas will see broad lines with a significant contribution from velocities considerably lower than V_s for a C-type shock and relatively narrow lines at velocities of $\sim \pm V_s$ for a J-type shock (cf. Hollenbach 1997). The overall shape of the SiO line profiles in BHR 71 hints then for the presence of C-type shocks. Regarding the spatial distribution, the large extent of the SiO emission in BHR 71, comparable in size to that of the CO, is similar to that seen toward the blue lobe of the L1157 outflow and notably different from the L1448 and IRAS 03282+3025 outflows in which the SiO is enhanced along the axes of the molecular outflow and/or at their ends. The latter distribution is characteristic of outflows associated with supersonic jets in which the molecular enhancement is expected to be narrowly confined to the immediate vicinity of the bow shock generated by the fast jet as it entrains ambient molecular material.

The widespread distribution of SiO emission in the lobes of BHR 71, similar in extent to the CO emission that is thought to be comprised mostly of swept-up ambient gas, suggests that the chemical enhancement in this source takes place in a shell-like structure produced by the dynamical interaction between the ambient cloud and an underlying wide-angled wind or wind-driven shell. The observed shape of the line profile of the SiO emission gives further support to the hypothesis that the SiO emission arises from quiescent material that has been accelerated by the passage of a shock driven by the wind, producing a shell-like outflow, rather than from fast bullets ejected by the YSO and moving in the ambient cloud. The BHR 71 outflow would then be an example of the class of outflows driven by a less collimated wide-angle wind, with the molecular enhancement occurring in a large shocked shell, surrounding the wind bubble, formed as the wind ablates material from dense clumps in the surroundings. Toward the blueshifted lobe of BHR 71 there is a large cavity carved out by the outflow on the near side of the globule (Fig. 13 of Paper I). The amount of material available in this region for processing by the shocks has probably diminished, although it is clearly still sufficient to kinetically excite the rotational transitions of many molecular species. Figure 1 shows that although the blue lobe may be protruding out of the densest part of the globule (as shown by the optical image), there is still a large amount of moderately dense gas outside of the optical boundaries (as indicated by the ^{13}CO emission).

The existence of a supersonic jet toward BHR 71 might not be ruled out, however. In fact it has been suggested that most molecular outflow sources might have jetlike and shell-like structures simultaneously, with one structure dominating over the other depending on the evolutionary stage (Padman, Bence, & Richer 1997). High-resolution imaging of both the L1448 and L1157 outflows shows that close to the source the CO peaks in a shell-like structure, whereas the SiO remains essentially jetlike (Gueth, Guilloteau, & Bachiller 1996; Zhang et al. 1997). This feature may be the result of a wandering jet in L1157, but in L1448 it appears to be a result of prompt entrainment of material by the underlying jet (Bachiller et al. 1995). Some evidence for the presence of a jet in BHR 71 is provided by the high-velocity (flow velocity of ~ 70 km s^{-1}) component seen in SiO, which might be probing a more collimated component of the outflow. Molecular hydrogen observations in the near-infrared (NIR) at 2.12 μm show extensive emission along the axis of the BHR 71 outflow (Bourke 1994; Bourke et al. 1999), which may be the result of successive eruptive events from the vicinity of the YSO.

Toward the NW, the H_2 emission traces a curved, elongated structure that could indicate a wandering jet with multiple bow shocks along its length. However, toward the southeast the H_2 emission lies mainly outside the SiO blue lobe and seems to abruptly terminate at the inner edge of this lobe. The difference in the spatial distribution of SiO and H_2 could be attributed to multiple outflow episodes, with the shell-like outflow seen in SiO representing an older event than the jetlike H_2 events. In this view the SiO flow would then correspond to a coasting shell created during an earlier jet episode.

5.2. SiO *Enhancement*

The high abundance of SiO molecules seen in BHR 71, and other molecular outflows, is most likely due to the

injection into the gas phase by shocks of Si atoms and/or Si-bearing species. Once silicon is injected into the gas phase, chemical models based on ion-molecule reactions predict a large abundance of SiO molecules (Turner & Dalgarno 1977; Hartquist, Oppenheimer, & Dalgarno 1980). Models of the chemistry in regions behind fast dissociative shocks predict a substantial enhancement in the abundance of SiO molecules (Neufeld & Dalgarno 1989). In particular, for shocks with velocities of 60–80 km s^{-1} propagating in a gas with preshock density of 10^4 cm^{-3} (about the average density of the BHR 71 globule; Paper I) the predicted column densities of SiO molecules are ~ 2–4×10^{12} cm^{-2}, similar to those derived in the lobes of the BHR 71 flow. A major drawback with the application of dissociative shock models to the BHR 71 flow is its moderate outflow velocity (~ 28 km s^{-1}), since shock velocities less than ~ 50 km s^{-1} are not fast enough to dissociate molecules. It is possible, however, that the weak HV emission seen in SiO, likely to be associated with high-velocity jets, could be explained by this type of model.

C-type shocks appear to be the most promising to explain the bulk characteristics of the BHR 71 flow. In particular the synthesis of molecules from atoms and ions can be highly efficient behind nondissociative C-type shocks. In fact, the detection of profuse SiO emission from other highly collimated bipolar outflows with moderate outflow velocities (e.g., Bachiller et al. 1991; Mikami et al. 1992; Bachiller et al. 1995; Zhang et al. 1995), have triggered several theoretical works on the production of SiO behind C-type shocks. The main mechanism of injection of silicon is sputtering driven by neutral particle impact on charged grains (Draine 1995; Flower & Pineau des Forêts 1995; Schilke et al. 1997); although grain-grain collisions can be important for low-velocity shocks ($25 \lesssim V_s \lesssim 35$ km s^{-1}) in dense regions [$n(H_2) > 5 \times 10^5$ cm^{-3}; Caselli et al. 1997]. The sputtering of Si-bearing material can arise from either grain cores, namely, refractory grains that are composed of silicates and graphites, or from grain mantles (Schilke et al. 1997). The release of Si-bearing material from grain cores requires higher impact energies than the release from mantles; substantial erosion of ice mantles can occur in C-shocks with velocities of ~ 25 km s^{-1}, whereas shock speeds of ~ 55 km s^{-1} are required in order to significantly erode the grain cores by He impacts. The inclusion of heavier species, such as CO and H_2O, can significantly lower the impact energies required for the erosion of grain cores, so that shock velocities as low as 25 km s^{-1} can cause substantial erosion of the grain cores (Schilke et al. 1997). Although the models are still preliminary, most are able to explain the column densities of SiO observed in the gas phase of molecular outflows. In particular, for the physical parameters typical of star-forming regions Caselli et al. (1997) found that the gas-phase SiO abundance behind C-shocks is larger than that in the quiescent gas by more than 3 orders of magnitude.

Another possible explanation for the widespread distribution of SiO in the BHR 71 outflow is the relative long lifetime of gas-phase SiO with respect to the outflow age (estimated at $\sim 10^4$ yr in Paper I). SiO is removed from the gas phase via reactions with OH, and Herbst et al. (1989) have determined that the abundance of SiO is 2 orders of magnitude greater than SiO_2 (the product of SiO + OH), even after 3×10^5 yr, in regions applicable to the conditions in the BHR 71 region (their model 4), so that once formed, SiO is not quickly removed from the gas phase. Pineau des Forêts, Flower, & Chièze (1997) show that the abundance of SiO is still significant 10^4 yr after the passage of a shock, even taking into account reaccretion onto grains. So the widespread detection of SiO in the outflow may be an indication of its youth, suggested by its small dynamical lifetime (Paper I), and may indicate that heating of the lobes by shocks is sufficiently recent that there has not yet been time for radiative cooling to occur. Bachiller (1996) notes that SiO emission is generally only observed in the outflows from the youngest (class 0) YSOs, consistent with the above scenario.

5.3. CH_3OH *Enhancement*

We find that the [CH_3OH]/[CO] abundance ratio of the outflowing gas in the lobes of BHR 71 is greater than that of the quiescent ambient gas by factors of ~ 40. Similar enhancements in the abundance of methanol in other young bipolar outflows have been reported by Bachiller et al. (1995). These large methanol abundances cannot be solely explained in terms of gas-phase chemistry (Menten et al. 1988; Millar, Herbst, & Charnley 1991). At the low temperature of molecular clouds, CH_3OH is thought to be depleted from the gas phase by condensation onto cold mantles of dust grains. The composition of the mantles depends on the physical conditions of the ambient medium. In particular, in an atomic hydrogen–rich ambient medium such as that of molecular clouds, water and methanol are expected to be the two most abundant constituents of icy mantles surrounding silicate and carbonaceous grains (Tielens 1989). A natural explanation for the large increase of the abundance of CH_3OH in the gas phase would then be evaporation of ice mantles rich in CH_3OH molecules.

The interstellar processes by which molecular species are removed from the ices and returned to the gas phase are, however, still a matter of investigation. A potentially important result from laboratory measurements is that of Blake et al. (1991) who show that an amorphous H_2O:CH_3OH ice mixture when warmed to 120 K selectively injects methanol into the gas phase. In bipolar flows, the most likely source of heating is shocks, which can raise the temperature of the gas evaporating the icy organic mantles of the grains and returning this material to the gas phase (Tielens & Allamandola 1987; Brown, Charnley, & Millar 1992). In the shock models of Schilke et al. (1997) ice mantles are completely destroyed in the shocks, their components being transferred to the gas phase. However, the details of how the methanol ice is liberated or how much the abundance of methanol is increased in the gas phase have yet to be quantitatively investigated. The similarities between the spatial distribution of the CH_3OH and SiO emission in the BHR 71 flow suggest that the process that leads to the evaporation of ice mantles also leads to the release of SiO and/or SiO_2 into the gas phase. In grain surfaces silicon is likely to be found in the form of SiO_2.

5.4. HCO^+ *and* CS *Abundances*

Table 6 shows that the [HCO^+]/[CO] abundance ratio of the outflowing gas in BHR 71 is smaller than in the quiescent ambient medium, or in other dark clouds, by typically a factor of 20 (cf. Guélin, Langer, & Wilson 1982; Baudry et al. 1981; Wootten et al. 1978; Swade 1989; Blake et al. 1995; Frerking, Langer, & Wilson 1987). Theoretical models of gas-phase chemistry behind weak shocks propa-

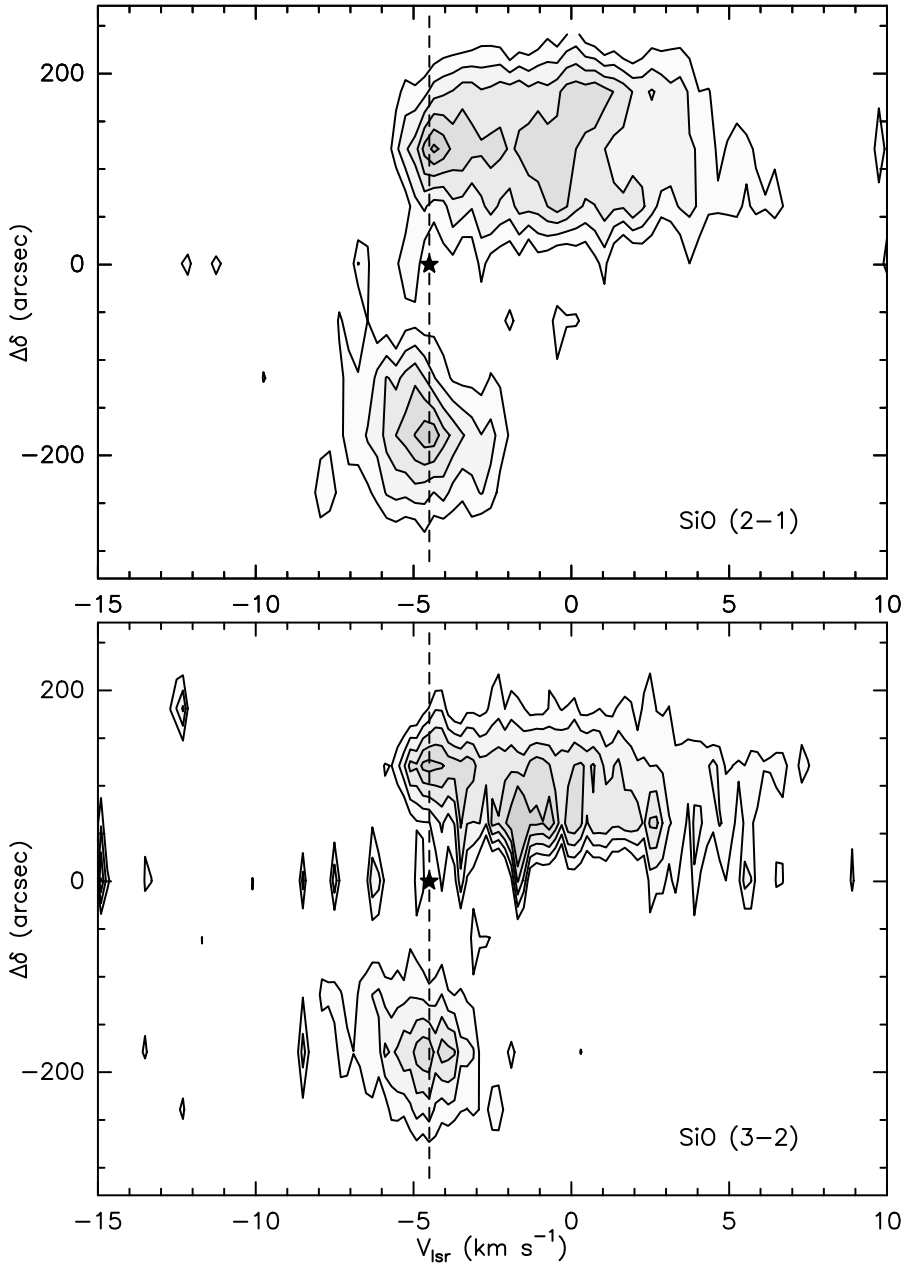

FIG. 7.—Position-velocity diagram of the SiO emission along the symmetry axis of the outflow. *Top:* SiO ($J = 2 \rightarrow 1$); contour levels are 0.075 to 0.5 by 0.05 K in T_A^*. *Bottom:* SiO ($J = 3 \rightarrow 2$); contour levels are 0.075 to 0.3 by 0.05 K in T_A^*.

gating into dense gas predict that the abundance of molecules such as HCO^+, CN, and H_2CO should decrease with respect to the preshock abundances, whereas the abundances of molecules such as CO are unperturbed (Iglesias & Silk 1978; Mitchell 1987; Bergin et al. 1998). In particular, Iglesias & Silk (1978) find that for a 10 km s^{-1} shock propagating into a cloud with a preshock density of 10^4 cm^{-3}, the abundance of HCO^+ should decrease by a factor of ~ 20, whereas Bergin et al. (1998) find that for a 20 km s^{-1} shock propagating into a cloud with a preshock density of 10^5 cm^{-3} and kinetic temperature of 30 K, the HCO^+ abundance should decreased by about a factor of 50. The low values of the $[HCO^+]/[CO]$ abundance ratio in the lobes of BHR 71 are consistent with the results predicted by shock models.

The [CS]/[CO] abundance ratios in the BHR 71 lobes are, on the other hand, similar to that of dark clouds, within the range of 10^{-5} to 10^{-4} (cf. Swade 1989; Fuller 1989; Irvine, Goldsmith, & Hjalmarson 1987; Lemme et al. 1995), suggesting that the abundance of the CS species is unperturbed or only slightly enhanced by the shock. In the few cases where the CS abundance in outflows from young stars has been estimated (e.g., Tafalla et al. 1997; Plambeck & Snell 1995; Takano 1986), an enhancement of a few is suggested, if any. A similar result is found for the shocked molecular cloud IC 443 (e.g., Ziurys, Snell, & Dickman 1989). This is in agreement with the few models that exist for the chemistry of CS in shocks (e.g., Pineau des Forêts et al. 1993; Leen & Graff 1988), which predict that the CS abundance remains essentially constant.

5.5. *The Low-Velocity Emission*

As mentioned earlier, in addition to the wing emission detected toward the lobes of BHR 71 in the lines of SiO and

CH_3OH, we also detect emission at velocities comparable to the systemic velocity of the globule. In particular for silicon monoxide, emission in the velocity range of the ambient cloud is clearly detected at the position of the lobes and barely visible toward the core. This can be appreciated in Figure 7, which shows velocity-position diagrams of the emission in the SiO lines along the symmetry axis of the outflow. The emission in the red lobe is roughly constant with velocity, with peaks at -4.1 and -0.8 km s^{-1}, whereas in the blue lobe the emission peaks at a velocity of -5.0 km s^{-1}, close to the ambient cloud velocity. This result might suggest that the low-velocity emission originates in a stationary quiescent ambient gas that has not been disturbed by the passage of a shock. The enhancement of SiO and CH_3OH molecules would then be due to two different processes: (1) heating of grains within the ambient medium by a radiation field able to evaporate volatile grain mantles and trigger gas-phase reactions, and (2) direct shock processing of dust located within the shocked region. Possible sources of heating of the ambient gas are radiation fields from shocks (Wolfire & Königl 1991, 1993; Taylor & Williams 1996), X-rays emitted by the protostar (e.g., Sekimoto et al. 1997), and/or UV photons generated in the accretion disk surrounding the protostar (Spaans et al. 1995).

6. SUMMARY

We have observed the highly collimated BHR 71 bipolar outflow in the $J = 3 \rightarrow 2$ and $J = 2 \rightarrow 1$ transitions of SiO and CS, the $J_k = 3_k \rightarrow 2_k$ and $J_k = 2_k \rightarrow 1_k$ transitions of CH_3OH, and the $J = 1 \rightarrow 0$ transition of HCO^+, using the SEST telescope. Broad wing emission was detected toward the outflow lobes in all the observed molecular transitions. The shape of the profiles are notably different from molecule to molecule depending on the relative intensities between a narrow line feature (arising from the ambient cloud in CS and HCO^+) and the broad component arising from the outflowing gas. Particularly striking are the cases of methanol and silicon monoxide molecules, for which the emission from the broad component is much stronger than that from the narrow component. Methanol lines exhibit the most intense wing emission, which suggests that these lines are powerful signposts of the chemical impact of bipolar outflows on the surrounding ambient medium.

The spatial distribution of the integrated wing emission is broadly similar in all the observed molecular transitions, showing well-separated blueshifted and redshifted lobes. The extent of the lobes in the SiO and CH_3OH lines, of $\sim 0.14 \times 0.08$ pc, are similar to those of the CO lobes, perhaps indicating a common mechanism for the excitation of these molecular lines. The SiO and CH_3OH profiles observed toward the red (blue) lobe are characterized by showing a broad wing emission with a maximum at a velocity close to the ambient cloud velocity, a gradual decrease in intensity from the peak velocity toward more redshifted (blueshifted) velocities, and a rapid decline in intensity toward the ambient cloud velocity. This spectral shape suggests that a small fraction of the molecular gas is accelerated to shock velocities, whereas the majority remain close to the ambient cloud velocity, and is characteristic of standard C-type shocks (Hollenbach 1997). The line profile shape, together with the extended spatial distribution, of the SiO and CH_3OH emission suggests that C-shocks created by the interaction between the surrounding ambient medium and a wide-angle wind or wind-driven shell, rather that a protostellar jet, play a major role in the production of these molecules toward the BHR 71 outflow. The intensity of the emission in the red lobe is typically ~ 2 times stronger than that toward the blue lobe, and the line widths are broader, which is probable due to environmental effects rather than intrinsic to the outflow mechanism.

We find that the abundance of methanol and silicon monoxide in the outflow lobes is enhanced with respect to that of typical dark clouds by factors of up to ~ 40 and 350, respectively, showing that these species are dramatically affected by the shocks. It appears that in the BHR 71 outflow the molecular enhancement takes place in a shell-like structure of swept-up material driven by a wind, rather than by a protostellar jet. The associated shocks cause the evaporation of icy grain mantles resulting in the injection into the gas phase of large amount of ice mantle constituents, such as methanol. Further, the shock seems to be sufficiently powerful that refractory dust grains are partially destroyed, liberating into the gas phase a significant amount of Si atoms that are later converted to SiO by ion-molecule reactions and/or shock chemistry.

Our multiline molecular observations also reveal that the $[HCO^+]/[CO]$ abundance ratios of the outflowing gas in BHR 71 are smaller than in quiescent dark clouds by typically a factor of 20, which can be interpreted as a result of shock chemistry. The [CS]/[CO] abundance ratios are, on the other hand, similar to that of dark clouds, suggesting that the abundance of the CS species is unperturbed by the shock. Finally, we suggest that the SiO and CH_3OH emission detected toward the lobes might not only trace shocked outflowing gas but also quiescent ambient gas that has been heated by UV and X-ray radiation produced by either the shocks themselves, the protostar, and/or an accretion disk.

G. G. gratefully acknowledges support from a Chilean Presidential Science Fellowship and from the Chilean Fondecyt Project 1980660. T. L. B. thanks the School of Physics, ADFA, and the SAO Predoctoral Fellowship program for financial support. We thank Malcolm Walmsley for providing the methanol code used in this paper, Ted Bergin for valuable discussions on the methanol zoo, and René Plume for his CS LVG code. This research has made use of NASA's Astrophysics Data System Abstract Service.

REFERENCES

André, P. 1995, Ap&SS, 224, 29
Avery, L. W., & Chiao, M. 1996, ApJ, 463, 642
Bachiller, R. 1996, ARA&A, 34, 111
Bachiller, R., Cernicharo, J., Martín-Pintado, J., Tafalla, M., & Lazareff, B. 1990, A&A, 231, 174
Bachiller, R., Liechti, S., Walmsley, C. M., & Colomer, F. 1995, A&A, 295, L51
Bachiller, R., Martín-Pintado, J., & Fuente, A. 1991, A&A, 243, L21
Bachiller, R., & Pérez Gutiérrez, M. 1997, in IAU Symp. 182, Herbig-Haro Flows and the Birth of Low Mass Stars, ed. B. Reipurth & C. Bertout (Dordrecht: Reidel), 153
Bachiller, R., Tereby, S., Jarrett, T., Martín-Pintado, J., Beichman, C. A., & van Buren, D. 1994, ApJ, 437, 296
Baudry, A., Perault, M., de La Noe, J., Despois, D., & Cernicharo, J. 1981, A&A, 104, 101
Bergin, E. A., Melnick, G. J., & Neufeld, D. A. 1998, ApJ, 499, 777

Blake, D., Allamandola, L., Sandford, S., Hudgings, D., & Freund, F. 1991, Science, 254, 548
Blake, G. A., Sandell, G., van Dishoeck, E. F., Groesbeck, T. D., Mundy, L. G., & Aspin, C. 1995, ApJ, 441, 689
Blake, G. A., Sutton, E. C., Masson, C. R., & Phillips, T. G. 1987, ApJ, 315, 621
Bourke, T. L. 1994, MSc thesis, Univ. New South Wales
Bourke, T. L., Hyland, A. R., & Robinson, G. 1995a, MNRAS, 276, 1052
Bourke, T. L., Hyland, A. R., Robinson, G., James, S. D., & Wright, C. M. 1995b, MNRAS, 276, 1067
Bourke, T. L., et al. 1997, ApJ, 476, 781 (Paper I)
———. 1999, in preparation
Brown, P. D., Charnley, S. B., & Millar, T. J. 1992, in Chemistry and Spectroscopy of Interstellar Molecules, ed. N. Kaifu (Tokyo: Univ. Tokyo Press), 149
Cabrit, S., & Bertout, C. 1990, ApJ, 348, 530
Caselli, P., Hartquist, T. W., & Havnes, O. 1997, A&A, 322, 296
Chiar, J. E., Adamson, A. J., Kerr, T. H., & Whittet, D. C. B. 1995, ApJ, 455, 234
Draine, B. J. 1995, A&AS, 233, 111
Flower, D. R., & Pineau des Forêts, G. 1995, MNRAS, 275, 1049
Frerking, M. A., Langer, W. D., & Wilson, R. W. 1987, ApJ, 313, 320
Fuller, G. A. 1989, Ph.D. thesis, Univ. California Berkeley
Guélin, M., Langer, W. D., & Wilson, R. W. 1982, A&A, 107, 107
Gueth, F., Guilloteau, S., & Bachiller, R. 1996, A&A, 307, 891
Hartquist, T. W., Oppenheimer, M., & Dalgarno, A. 1980, ApJ, 236, 182
Herbst, E., Millar, T. J., Wlodek, S., & Bohme, D. K. 1989, A&A, 222, 205
Hollenbach, D. 1997, in IAU Symp. 182, Herbig-Haro Flows and the Birth of Low Mass Stars, ed. B. Reipurth & C. Bertout (Dordrecht: Reidel), 181
Iglesias, E. R., & Silk, J. 1978, ApJ, 226, 851
Irvine, W. M., Goldsmith, P. F., & Hjalmarson, A. 1987, in Interstellar Processes, ed. D. J. Hollenbach & H. A. Thronson (Dordrecht: Reidel), 561
Leen, T. M., & Graff, M. M. 1988, ApJ, 325, 411
Lemme, C., Walmsley, C. M., Wilson, T. L., & Muders, D. 1995, A&A, 302, 509
Linke, R. A., Frerking, M. A., & Thaddeus, P. 1978, ApJ, 234, L139
Menten, K. M., Walmsley, C. M., Henkel, C., & Wilson, T. L. 1988, A&A, 198, 253
Mikami, H., Umemoto, T., Yamamoto, S., & Saito, S. 1992, ApJ, 392, L87
Millar, T. J., Herbst, E., & Charnley, S. B. 1991, ApJ, 369, 147
Mitchell, G. F. 1987, in IAU Symp. 120, Astrochemistry, ed. M. S. Vardya & S. P. Tarafdar (Dordrecht: Reidel), 275
Mundy, L. G., Snell, R. L., Evans, N. J., Goldsmith, P. F., & Bally, J. 1986, ApJ, 306, 670
Neufeld, D. A., & Dalgarno, A. 1989, ApJ, 340, 869
Padman, R., Bence, S., & Richer, J. 1997, in IAU Symp. 182, Herbig-Haro Flows and the Birth of Low Mass Stars, ed. B. Reipurth & C. Bertout (Dordrecht: Reidel), 123
Pineau des Forêts, G., Flower, D. R., & Chièze, J.-P. 1997, in IAU Symp. 182, Herbig-Haro Flows and the Birth of Low Mass Stars, ed. B. Reipurth & C. Bertout (Dordrecht: Reidel), 200
Pineau des Forêts, G., Roueff, E., Schilke, P., & Flower, D. R. 1993, MNRAS, 262, 915
Plambeck, R. L., & Snell, R. L. 1995, ApJ, 446, 234
Raga, A. C., & Cabrit, S. 1993, A&A, 278, 267
Sandqvist, A. 1977, A&A, 57, 467
Schilke, P., Walmsley, C. M., Pineau des Forêts, G., & Flower, D. R. 1997, A&A, 321, 293
Sekimoto, Y., Tatematsu, K., Umemoto, T., Koyama, K., Tsuboi, Y., Hirano, N., & Yamamoto, S. 1997, ApJ, 489, L63
Snell, R. L., Mundy, L. G., Goldsmith, P. F., Evans, N. J., & Erikson, N. R. 1984, ApJ, 276, 625
Spaans, M., Hogerheijde, M. R., Mundy, L. G., & van Dishoeck, E. F. 1995, ApJ, 455, L167
Swade, D. L. 1989, ApJ, 345, 828
Tafalla, M., & Bachiller, R. 1995, ApJ, 443, L37
Tafalla, M., Bachiller, R., Wright, C. H., & Welch, W. J. 1997, ApJ, 474, 329
Takano, T. 1986, ApJ, 300, L85
Taylor, S. D., & Williams, D. A. 1996, MNRAS, 282, 1343
Tielens, A. G. G. M. 1989, in Interstellar Dust, ed. L. J. Allamandola & A. G. G. M. Tielens (Dordrecht: Kluwer), 239
Tielens, A. G. G. M., & Allamandola, L. J. 1987, in Physical Processes in Interstellar Clouds, ed. G. E. Morfill & M. Scholer (Dordrecht: Reidel), 333
Turner, J. L., & Dalgarno, A. 1977, ApJ, 213, 386
van Dishoeck, E. F., & Blake, G. A. 1995, Ap&SS, 224, 237
van Dishoeck, E. F., Blake, G. A., Draine, B. T., & Lunine, J. I. 1993, in Protostars and Planets III, ed. E. H. Levy & J. Lunine (Tucson: Univ. Arizona Press), 163
Vrtilek, J. M., Gottlieb, C. A., & Thaddeus, P. 1987, ApJ, 314, 716
Whittet, D. C. B., Adamson, A. J., Duley, W. W., Geballe, T. R., & McFadzean, A. D. 1989, MNRAS, 241, 707
Wolfire, M. G., & Königl, A. 1991, ApJ, 383, 205
———. 1993, ApJ, 415, 204
Wootten, A., Evans, N. J., Snell, R., & Vanden Bout, P. 1978, ApJ, 225, L143
Zhang, Q., Ho, P. T. P., Wright, M. C. H., & Wilner, D. J. 1995, ApJ, 451, L71
———. 1997, in IAU Symp. 182, Poster Proceedings, Low Mass Star Formation from Infall to Outflow, ed. F. Malbet & A. Castets (Grenoble: Observatiore de Grenoble)
Ziurys, L. M., Snell, R. L., & Dickman, R. L. 1989, ApJ, 341, 857